Exploiting vitamin C as a prooxidant to activate ROS-responsive prodrugs for potent and selective tumor killing

Taufeeque Ali,[1] Thilini Nimasha Fernando Ponnamperumage,[1] Alexis Kimberly Peterson,[1] Daniel Li,[1] Hanlun Gao,[1] Jatin Pandey,[1] Julia Anna Rose Jakusz,[1] Heli Fan,[1] Gilbert Edward Koelsch,[1] Leggy A. Arnold,[1] Julie M. Jorns,[2] Yee Chung Cheng,[3] Avik Roy,[4] Gang Zhou,[5] and Xiaohua Peng[1,*]

[1]Department of Chemistry and Biochemistry and the Milwaukee Institute for Drug Discovery, University of Wisconsin-Milwaukee, 3210 N. Cramer Street, Milwaukee, Wisconsin, 53211, United States

[2]Department of Pathology, Medical College Wisconsin, Milwaukee, Wisconsin

[3]Department of Hematology and Oncology and Department of Medicine, Medical College Wisconsin, Milwaukee, Wisconsin

[4]Research and Development Laboratory, Simmaron Research Institute, Milwaukee, WI, USA

[5]Georgia Cancer Center, Medical College of Georgia, Augusta University, Augusta, GA, USA

[*]To whom correspondence may be addressed. Email: pengx@uwm.edu

Abstract

Developing targeted cancer therapy with minimal side effects remains a significant challenge. Oxidative stress-based cancer therapies have gained traction in recent years. However, challenges such as limited tumor selectivity and therapeutic durability often hinder their clinical application. Here, we report a novel strategy of combining ROS-responsive prodrugs with prooxidants to achieve potent, durable, and selective tumor killing effects. This approach leverages pro-oxidants (i.e. ascorbate) to amplify oxidative stress within tumors, sensitizing cancer cells to ROS-responsive prodrugs. Both *in vitro* and *in vivo* studies confirm the anticancer synergism and selectivity of this combination therapy, which achieved complete tumor regression without recurrence, significantly outperforming single-agent treatments. This combination therapy is effective against hard-to-treat cancers like triple-negative breast cancer and glioblastoma. Our findings highlight the potential of targeting tumor redox mechanisms through a combination of ROS-responsive prodrugs and pro-oxidants, offering a promising avenue for repurposing these agents in cancer therapy.

Keywords: combination therapy, synergistic anticancer effects, ROS-responsive prodrugs, triple negative

breast cancer, ROS-generating agents, vitamin C, complete tumor regression

1. Introduction

Cancer cells exhibit elevated oxidative stress due to oncogene activation, tumor suppressor gene inactivation, increased metabolism, and diminished antioxidant activities.(*1-4*) Consequently, cancer cells tend to have higher basal level of reactive oxygen species (ROS) than normal cells. This feature has been exploited to develop therapeutic strategies that selectively target cancer cells while sparing normal cells. One such strategy, known as oxidative stress-based cancer therapy, is to use pro-oxidants to drive ROS production and accumulation to an excessive level in cancer cells, resulting in irreversible damages to DNA, proteins and lipids that lead to eventual cell death. Numerous pro-oxidants have been identified for their ability to induce oxidative stress in cancer cells, showing promising results in certain cases.(*2-11*) However, the application of oxidative stress-inducing pro-oxidants for cancer treatment faces many challenges, including limited tumor-selectivity, dose-limiting toxicity, inefficient drug delivery, acquired resistance, etc.

The feature that cancer cells have elevated levels of ROS compared to normal cells has also been employed to develop a class of prodrugs that only become cytotoxic in the presence of ROS such as hydrogen peroxide (H_2O_2)(*12-23*). We have recently developed a group of prodrugs by coupling DNA alkylating agents with arylboronate or boronic acid, which can be activated by high H_2O_2 levels in cancer cells.(*17, 18, 24-26*) These compounds remain inactive until entering cancer cells, where elevated H_2O_2 levels convert them into potent alkylating agents. Among these, **FAN-NM-CH$_3$** has emerged as a promising candidate with favorable drug-like properties.(*25*) (Fig. 1) Although ROS-activated prodrugs hold the promise of improving tumor selectivity and reducing adverse drug reactions, their use as single-agent therapy has met some obstacles, including ROS heterogeneity in tumor cells, insufficient activation of the prodrugs, and limited therapeutic durability. Novel strategies are needed to overcome these hurdles to fully capitalize the therapeutic potential of ROS-activated prodrugs.

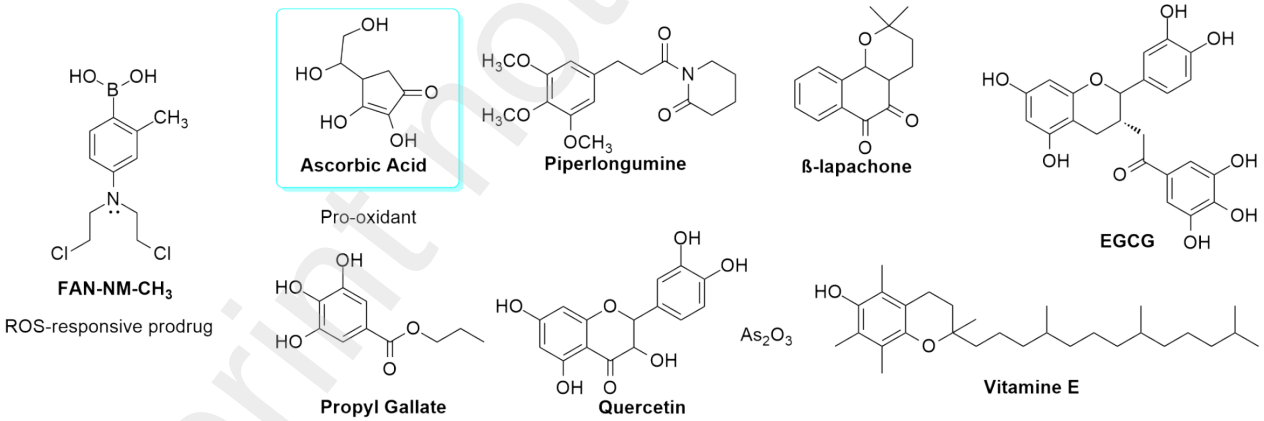

Fig. 1. **ROS-responsive prodrug and pro-oxidants tested in combination therapy**.

In this study, we set out to test whether combining ROS-activated prodrugs with pro-oxidants can achieve selective, potent and durable tumor killing. This novel approach is based on the rationale that the ROS-amplifying effect of a pro-oxidant can fully activate a ROS-responsive prodrug in cancer cells to mediate tumor destruction more effectively than either drug alone. Here, we screened a panel of compounds with pro-oxidant activities and identified vitamin C (**vitC**, ascorbate) as an attractive candidate compatible with our lead ROS-responsive prodrug **FAN-NM-CH$_3$** to exert synergistic anticancer effect both *in vitro* and

in vivo). We reveal that the efficacy and tumor selectivity of this combinatory regimen relies on **vitC**-induced H_2O_2 production and tumor-intrinsic deficiency in catalase activity. Our results provide proof of concept for a novel and effective approach that targets tumor redox for cancer treatment.

2. Materials and methods

2.1. Cell Culture

The human tumor cell lines MDA-MB-468 (HTB-132), MCF7 (HTB-22), MDA-MB-436 (HTB-130), MDA-MB-231 (HTB-26) and normal cell lines HMEC (PCS-600-010), MCF 10A (CRL-10317) were purchased from the American Type Culture Collection. U-87 MG cells were generously provided by Dr. Shama Mirza (Shimadzu Laboratory). MDA-MB-468, MDA-MB-436, and MDA-MB-231 cells were cultured in L-15 Leibovitz media (Thermo Scientific Catalog: 41300070) supplemented with 10 % fetal bovine serum (FBS, Biowest: S1620), 1% non-essential amino acids (NEAA 100X solution, HyClone no: SH30238.01), and 1% penicillin and streptomycin (HyClone Penicillin Streptomycin 100X Solution, HyClone no: SV30010) at 37 °C in 100% relative humidity. MCF7 and U-87 MG cells were maintained in ATCC-formulated Eagle's Minimum Essential Medium (30-2003) supplemented with 10 % fetal bovine serum (FBS, Biowest: S1620). 1% penicillin and streptomycin (HyClone Penicillin Streptomycin 100X Solution, HyClone no: SV30010) and 0.01 mg/mL human recombinant insulin (Sigma Aldrich Inc: 91077C) was added to MCF7 media. HMEC cells were maintained in Mammary Epithelial Cell Growth Media Kit (PCS-600-030, PCS-600-040) from ATCC. MCF 10A cells were maintained in Lonza media kit MEGM (CC-3150) supplemented with 100 ng/mL Cholera toxin. MCF7, U-87 MG, HMEC, and MCF 10A cells were maintained in 5% CO_2 incubator at 37 °C.

2.2. Reagents and Assay kits

The reagents used in this study includes Ascorbic Acid (VWR: BDH9242-100G), (-)-Epigallocatechin Gallate Hydrate (TCI America: 989-51-5), Piperlongumine (Indofine Chemical Co: 20069-09-4), Propyl Gallate (Mp Biomedicals Inc: 121-79-9), Quercetin (Asta Tech Inc: 117-39-5), Vitamin E (Santa Cruz Biotechnology: 10191-41-0), Arsenic (III) oxide (SIAL: 1327-53-3), β-Lapachone (Ambeed: 4707-32-8), Chlorambucil (Sigma-Aldrich: 305-03-3), Corning Matrigel (Corning: 354248), and Catalase (Sigma-Aldrich: C3155-100MG). The Assay kits employed include Celltiter-Glo Reagent (Promega: G7570), Catalase Colorimetric Activity Kit (Invitrogen: EIACATC), Amplex Red Hydrogen Peroxide/Peroxidase Assay (Invitrogen, A22188), Dead Cell Apoptosis Kit with Annexin V Alexa Fluor 488 and Propidium Iodide (PI) (ThermoFisher Scientific: V-13245), DAPI solution (1 mg/mL) (ThermoFisher Scientific (62248), Hydrogen Peroxide Assay Kit (Cell-based) (abcam: ab138874), Alkaline Comet Assay Kit (abcam: ab238544), IRDye 800CW 2-DG Optical Probe (LI-COR: 926-08946), and ROS Brite 700 probe (ATT Bioquest: 16004).

2.3. Cytotoxicity assay

Cells were plated into 96-well optical bottom plates (Nunc: 1256671) in 40 µL media at densities ranging from 3,000 to 5,000 cells/well. The plates were incubated for 3 h prior to the addition of the compounds. *IC_{50} determination*: **FAN-NM-CH_3**, Chlorambucil, Piperlogumine, β-Lapachone, Vitamin E, Propyl Gallate, Quercetin, and EGCG were solubilized in dimethyl sulfoxide (DMSO) at 20 mM stock. Arsenic Trioxide and **vitC** were dissolved in DI H_2O. Arsenic stock was 20 mM and **vitC** was dissolved at 1 M with pH adjusted to 7.0 with 1 M NaOH solution. All stocks were serially diluted (2-fold, 11 times). 400 nL of the serially diluted stocks were added to the cell plate (1:100 dilution) using a Tecan Freedom EVO liquid handling system equipped with a 100 nL pin tool (V&P Scientific). **FAN-NM-CH_3** *IC_{50} curve in combination with prooxidants:* Prooxidants Piperlongumine, β-Lapachone, Vitamin E, Propyl Gallate, Quercetin, and EGCG were solubilized in DMSO at 312 µM, 312 µM, 624 µM, 10 mM, 1.25 mM, and 5

mM stock respectively. Arsenic trioxide and **vitC** were dissolved in DI H_2O. Arsenic stock was 316 µM and **vitC** was dissolved at 400 mM with pH adjusted to 7.0 with 1 M NaOH solution. 100 nL of the stocks were added to the assay plates (1:400 dilution) 1 h prior to the addition of the **FAN-NM-CH_3**, using a Tecan Freedom EVO liquid handling system equipped with a 100 nL pin tool (V&P Scientific). **FAN-NM-CH_3** was solubilized in DMSO at 20 mM stock. This stock was serially diluted (2-fold, 11 times), 400 nL of the serially diluted stocks was added to the same assay plates (1:100 dilution) using a Tecan Freedom EVO liquid handling system equipped with a 100 nL pin tool (V&P Scientific). *Dose response:* 7 µM Catalase solution (Sigma-Aldrich: C3155-100MG) was diluted 10-fold in Millipore water. 4 µL of the diluted catalase solution was added to the cell plate (1:10). Plates were incubated for 1 h prior to the addition of **vitC**. MDA-MB-468, MCF7, U87, and MCF 10A received 100 nL (1:400) of the 400 mM, 100 mM, 120 mM, and 400 mM stocks of **vitC** in DI H_2O respectively (**vitC** pH was adjusted to 7.0 with NaOH). Plates were then incubated for another hour prior to the addition of **FAN-NM-CH_3**. 100 nL of 400 µM, 800 µM, 2 mM, and 400 µM stocks of **FAN-NM-CH_3** in DMSO was added to each MDA-MB-468, MCF7, U87, and MCF 10A assay plates respectively. All plates were incubated for an additional 48 h followed by the addition of 40 µL of Celltiter-Glo Reagent (Promega). Luminescence was measured after 30 minutes of incubation using an Infinite M1000 (Tecan) plate reader. Normalized % viability was assessed for each concentration against the individual vehicle treatments (DMSO or DI H_2O).

2.4. Determination of Combination Index and Dose Reduction Index

The Chau-Talalay interaction combination index (CI) and dose reduction index (DRI),(*27, 28*) commonly used to determine the synergistic effect between two drugs, were calculated as follows:

$$CI = \left(\frac{D1}{Dx1}\right) + \left(\frac{D2}{Dx2}\right)$$

$$DRI\ 1 = \left(\frac{Dx1}{D1}\right)$$

$$DRI\ 2 = \left(\frac{Dx2}{D2}\right)$$

where Dx1 and Dx2 represent the doses of **FAN-NM-CH_3** and **vitC** required to inhibit cell growth by 50%, respectively, and D1 (**FAN-NM-CH_3**) and D2 (**vitC**) indicate the individual doses of the two drugs required for 50% inhibition of cell growth when used in combination. The combined effects of the two drugs are indicated as follows:

$$CI < 1\ (Cooperative\ effect), CI = 1\ (additive\ effect), and\ CI > 1\ (antagonistic\ effect)$$

A higher DRI value indicates a reduced drug dosage is needed in combination to achieve the same efficacy as a single drug.

2.5. Synergy Evaluation by SynergyFinder 3.0

Cell viability was measured following a 48-hour treatment period using the CellTiter-Glo assay. The percentage of viable cells relative to untreated control cells was determined to assess the cytotoxic effects of **vitC**, **FAN-NM-CH_3**, and their combinations. Pairs of drugs were tested in combination at five serially diluted concentrations with a sixth concentration serving as a control. **vitC** was tested at concentrations ranging from 0 µM to 4000 µM, and **FAN-NM-CH_3** was tested at concentrations ranging from 0.5 µM to

5 μM. Each combination and individual drug treatment was performed in at least three independent experiments per cell line. An excel matrix sheet was prepared containing Drug 1 and Drug 2 data with their corresponding percentage of viable cells relative to the untreated control, formatted for input into SynergyFinder. The SynergyFinder 3.0 platform (https://synergyfinder.fimm.fi/) was used to calculate and visualize synergy scores.(*29*) The Bliss Independence model was primarily used to analyze the synergy as it evaluates drug interactions by assuming independent action of the drugs. Synergy scoring was visualized as 2D and 3D interaction surface over the dose matrix. The depth of color in the two-dimensional image and the height of the three-dimensional landscape indicated the degree of synergy, additivity, or antagonism among drug combinations.

2.6. Determination of Catalase Activity

Catalase activity was measured using the Catalase Colorimetric Activity Kit (Invitrogen: EIACATC) according to the manufacturer's instructions. Cells (1 x 10^5) were seeded in each well of 6-well tissue culture plates (VWR: 10062-892). Once the cells reached 90% confluency (~1 x 10^6 cells), they were treated with either no treatment, vehicle, **vitC**, **FAN-NM-CH$_3$**, or a combination of both. Plates were then incubated for 48 h prior to sample preparation. The media was removed, and cells were washed twice with 3 mL of ice-cold PBS (without Mg^{2+} and Ca^{2+}). Cells were gently dislodged using a rubber policeman, collected in 1.5 mL microcentrifuge tubes, and sonicated in 1 mL of cold 1X assay buffer. The samples were then centrifuged at 10,000 x g for 15 minutes at 4 °C, and the collected supernatants were normalized to 100 μg/mL of protein using Pierce Detergent compatible Bradford assay reagent (Thermo Scientific: 23246S). The collected samples were diluted 1:5 in 1X assay buffer. Catalase standards were prepared by diluting 10 μL of the catalase standard solution in 190 μL of 1X assay buffer to obtain a 5 U/mL catalase solution. This solution was further diluted 2-fold five times, including a blank with 1X assay buffer. Fresh standards were prepared 1-2 hours prior to use. 25 μL of the standards and diluted samples were added to the clear 96-well half-area plate provided with the kit, followed by 25 μL of Hydrogen Peroxide Reagent into each well. The plate was incubated for 30 minutes at room temperature. Subsequently, 25 μL of substrate and 25 μL of 1X HRP solution were added to each well. The plate was incubated at room temperature for 15 minutes. Absorbance was recorded at 560 nm using the Infinite M1000 (Tecan) plate reader. A standard curve was generated using curve-fitting on GraphPad Prism software, and the activity of unknown samples was calculated from the standard curve and adjusted for the appropriate dilution factor.

2.7. RNA extraction and RT-qPCR

Cells (1 x 10^5) were seeded in each well of 6-well tissue culture plates (VWR: 10062-892). Once the cells reached 90% confluency (~1 x 10^6 cells), they were treated with either vehicle, **vitC**, **FAN-NM-CH$_3$**, or a combination of both. Plates were then incubated for 48 h prior to sample preparation. Cells were harvested and resuspended in 350 μL of RLT buffer in the presence of 1% β-mercaptoethanol. QIAshredder spin columns (Qiagen: 79656) was used to lyse the cells and total isolated RNA was purified with RNAeasy kit (Qiagen: 74104). Quantification was done by reading absorbance (260 nm/280 nm) using Infinite M1000 (Tecan) plate reader. RNA was reverse transcribed into cDNA using qScript One-Step SYBR Green qRT-PCR Kit (QuantaBio: 95054-946). Primers used are as follows: GAPDH forward primer (FP) 5'-ACCACAGTCCATGCCATCAC-3', GAPDH reverse primer (RP) 5´-TCCACCACCCTGTTGCTGTA-3´; P53 FP 5'-GTTCCGAGAGCT GAATGAG-3', P53 RP 5'-TTATGGCGGGAGGTAGACTG-3'; Catalase FP 5'-CCAGAAGAAAGC GGTCAAGAA-3', Catalase RP 5'-GAGATCCGGACTGCACAAAG-3'. cDNA synthesis and amplification were done on an

Eppendorf Mastercycler in a 96-well twin.tec PCR plate (Eppendorf: 951022015). A 20 µL reaction volume comprised of 10 µL SYBRGreen Master Mix 2X, 4.8 µL RNase-Free water, 1 µL of each primer, 0.2 µL of RT, and 3 µL of RNA (50 ng) in each well. Melting curve was used to assess target specificity. The gene expressions were normalized to relative GAPDH expression. Relative expression of each gene against their controls were calculated using the $2^{-\Delta\Delta Ct}$ method of Lovak and Schmittgen. Standard deviations were calculated for three biologically independent trials performed in triplicates.

2.8. Measurement of extracellular/intracellular H_2O_2 levels

Extracellular H_2O_2 levels were determined using an Amplex Red Hydrogen Peroxide/Peroxidase Assay (Invitrogen: A22188) and intracellular H_2O_2 levels were determined using Hydrogen Peroxide Assay Kit (abcam: ab138874) as per their respective manufacturer's protocol. Briefly $25x10^3$-$50x10^3$ cells were seeded in each well of a 96 Well Black, Optically Clear Polymer Bottom Plate (Thermo Scientific™ Catalog: 1256670) in 40 µL (Final reaction volume). The plates were incubated for 3 h prior to the addition of the compounds. *Ascorbic acid dose-dependent H_2O_2 detection:* **vitC** was dissolved in DI H_2O at 1 M stock concentration and pH adjusted to 7.0 using 1 M Sodium Hydroxide solution. The stock was serially diluted (2-fold, 11 times). 400 nL of these serially diluted stocks were added to the cell plate (1:100 dilution) using a Tecan Freedom EVO liquid handling system equipped with a 100 nL pin tool (V&P Scientific). *Dose response:* A 7 µM Catalase solution (Sigma-Aldrich: C3155-100MG) was diluted 10-fold in Millipore water. 4 µL of the diluted catalase solution was added to the cell plate (1:10). Plates were incubated for 1 h prior to the addition of **vitC**. MDA-MB-468, MCF7, U87, and MCF 10A received 100 nL (1:400) of the 400 mM, 100 mM, 120 mM, and 400 mM stocks of **vitC** in DI H_2O respectively (**vitC** pH was adjusted to 7.0 with sodium hydroxide). Plates were then incubated for another hour prior to the addition of **FAN-NM-CH_3**. 100 nL of 400 µM, 800 µM, 2 mM, and 400 µM stocks of **FAN-NM-CH_3** in DMSO were added to each MDA-MB-468, MCF7, U87, and MCF 10A assay plates respectively. All Plates were incubated for an additional 48 h. *Controls:* All controls were freshly prepared using ~3% Hydrogen peroxide (comes with each kit) in 1X KRPG buffer (Krebs–Ringer phosphate consists of 145 mM NaCl, 5.7 mM sodium phosphate, 4.86 mM KCl, 0.54 mM $CaCl_2$, 1.22 mM $MgSO_4$, 5.5 mM glucose, pH 7.35) prior to assaying. *Extracellular H_2O_2 levels:* After 48 h incubation, the cells were washed twice with 1X KRPG buffer and incubated for 5 h in 40 µL KRPG buffer. Then, 20 µL of this KRPG buffer was transferred into another 96 Well Black, Optically Clear Polymer Bottom Plate (Thermo Scientific™ Catalog: 1256670) in triplicates and mixed with an equal amount of Amplex Red reagent (50 µM Amplex Red and 0,1 U/mL HRP final concentrations). After 5 h incubation, fluorescence was measured (Ex/Em: 560/590 nm) on an infinite M1000 (Tecan) microplate reader. Note that the final concentration of H_2O_2 controls has been adjusted to account for the dilution by the same volume of Amplex Red reagent. *Intracellular H_2O_2 levels:* After 48 h incubation, the cells were washed twice with 1X KRPG buffer. 40 µL of 1X AbGreen in assay buffer was added to each well. Plates were incubated for 60 minutes at room temperature in dark. Fluorescence was measured (Ex/Em: 490/520) on an infinite M1000 (Tecan) microplate reader. The same plates were used for fluorescence microscopic imaging on an EVOS Digital Inverted Microscope.

2.9. Detection of Cell Apoptosis

Apoptosis was assessed using Dead Cell Apoptosis Kit with Annexin V Alexa Fluor 488 with Propidium Iodide (PI) (ThermoFisher Scientific: V-13245), and DAPI solution (1 mg/mL) (ThermoFisher Scientific (62248) as per manufacturer's protocol. $50x10^3$ cells were seeded in each well of the Thermo Scientific Nunc Lab-Tek II chamber slide (Thermo Scientific: 125658) with a final reaction volume of 500 µL and incubated for 3 h prior to the treatment. MDA-MB-468, MCF7, U87, and MCF 10A received 1.25 µL

(1:400) of the 400 mM, 100 mM, 120 mM, and 400 mM stocks of **vitC** in DI H_2O respectively (**vitC** pH was adjusted to 7.0 with sodium hydroxide). Plates were then incubated for another hour prior to the addition of **FAN-NM-CH$_3$**. 1.25 µL of 400 µM, 800 µM, 2 mM, and 400 µM stocks of **FAN-NM-CH$_3$** in DMSO were added to each MDA-MB-468, MCF7, U87, and MCF 10A assay plates respectively. All Plates were incubated for an additional 48 h. After the treatment, cells were washed with ice-cold PBS twice. After the wash, 20 µL of the Annexin V and 2 µL of the 100 µg/mL PI stock in 78 µL 1X Annexin binding buffer was added to each well with a final reaction volume of 100 µL. The chamber slides were incubated for 30 minutes and washed with a 1X Annexin binding buffer. A final wash was done with 1:500 dilution of the 1 mg/mL DAPI solution in PBS for 5 minutes. Chambers were detached and slides were mounted with the Fluoromount (TM) Aqueous Mounting Medium (Sigma-Aldrich: F4680) with a glass cover slip. The slides were kept in the dark and imaged the next day in the dark room on an Accu Scope EXC-500 Fluorescence microscope system.

2.10. Alkaline comet assays

The comet assay was performed according to manufacturer's protocol (Abcam: ab238544). Cells were seeded in 6-well tissue culture plates (VWR: 10062-892) at a density of $1x10^5$ cells. Once cells reached 90% confluency, they were treated at varied conditions for 48 h. Cells were gently removed from the 6-well plate with a rubber policeman in 1 mL ice-cold PBS (without Mg^{2+} and Ca^{2+}). Cells were isolated by centrifugation at 700 x g for 3 min. Supernatant was discarded. Cell pellet was washed again in ice-cold PBS. Finally, cells were resuspended in PBS and further diluted to 1 x 10^5 cells/mL. 180 µL of the preheated comet agarose maintain at 37 ℃ in water bath was gently mixed with 20 µL cell samples (1:10). 150 µL/well of this mix was transferred onto a pre-warmed glass and maintained horizontally for 5 min. Slides were then transferred to 4 ℃ in the dark for 30 min to let the agarose solidify. The slides were then transferred into a small basin containing pre-chilled lysis buffer at 4 ℃ for 2 h in the dark. The Lysis buffer was then replaced with pre-chilled alkaline unwinding solution (300 mM NaOH, 1 mM EDTA) in 4 ℃ for 30 min in the dark. The slides were then gently transferred into a horizontal electrophoresis chamber with pre-chilled alkaline electrophoresis solution (300 mM NaOH, 1 mM EDTA, pH > 13) and ran with a voltage of 35 V applied for 25 min. Slides were then slowly removed and rinsed with DI water twice for 2 min followed by cold 70% ethanol for 5 min. The slides were allowed to air dry in the dark for 1 h. 100 µL/well of diluted Vista Green DNA dye was added onto the agarose. The slides were then incubated at room temperature for 15 min in the dark. Comets were analyzed under an EVOS Digital Inverted Microscope at 20X magnification. DNA damage was quantified using TriTek CometScore Software.

2.11. Experimental Animals

Six-week-old female CD1 mice from Charles River Laboratory were used for a safety study, while immune-deficient female nude mice (Charles River Strain, Code 490) weighing 22−25 g were used for an *in vivo* efficacy study. The animals were housed under specific pathogen-free conditions, maintained under standard humidity, temperature, and a controlled 12-hour light/dark cycle, with free access to food and water. All animals were allowed to acclimate for approximately seven days before experimental procedures. All animal experiments complied with the University of Wisconsin−Milwaukee Institutional Animal Care and Use Committee (IACUC) guidelines.

2.12. Safety Study

The maximum tolerated dose (MTD), defined as the highest dose not causing a serious adverse event (e.g.,

death, convulsion, ataxia, aberrant behavior, or evident pain) observed within 2 d of observation, was determined for the prodrug and **vitC** among female CD1 mice using groups of three animals per group. **vitC** was dissolved in DI water and pH was adjusted to 7.0 with NaOH. 100 µL of this was administered intraperitonially. The prodrug was formulated in a mixture of DMSO, poly(ethylene glycol) (PEG) 400, and phosphate-buffered saline (PBS) (volume ratio 2:19:19). 1 h after the **vitC** injection, 100 µL of the prodrug was administered through IP. 3 mice per group were used. *Escalation Study:* Escalating IP dosages were administered of **vitC** (1 g/kg, 2 g/kg, 3 g/kg, and 4 g/kg) against fixed prodrug doses (5 mg/kg, 10 mg/kg, and 20 mg/kg) until serious adverse events were observed or the maximum dosage was reached (20 mg/kg prodrug in combination with 4g/kg **vitC**). Dose escalations were conducted with a one-day interval, and weights were documented on the second day. *5-dose Study:* To identify a safe dose of the **vitC** for an *in vivo* efficacy study, decreased doses of **vitC** (500 mg/kg, 750 mg/kg, and 1 g/kg) and the prodrug (5 mg/kg, 10 mg/kg, and 20 mg/kg) (IP injection) were given to the female CD-1 mouse (three mice for each dose) each day until a dose was administered with no signs of weight loss for all mice over a period of 5 d. Once the dosing was completed, animals were observed for another 2 d to observe delayed-onset toxicity effects. Animals with the following signs were euthanized: weight loss of 20% from the initial weight or more, the inability to rise, ambulate, or reach food and water for over 3 d, and the presence of a labored respiration.

2.13. In Vivo Efficacy Study with Xenograft Models

Seven-week-old Immune-deficient female nude mice were anesthetized with isoflurane and injected subcutaneously with cancer cells (MDA-MB-468) suspended in a 1:1 solution of Matrigel (Corning: 354248) and Dulbecco's Modified Eagle Medium (DMEM) media. All cancer cells were obtained from the American Type Culture Collection (ATCC) and were negative for bloodborne pathogens. Cell numbers for each inoculation (100 µL per mouse to the subcutaneous area of the flank) were $5x10^6$. Animals were monitored daily for palpable tumors, and animal weights were recorded weekly before/after the compound was administered. When the tumors reached treatment size (200 mm^3), the mice were randomized to treatment groups (4 groups with 3 mice per group). A vehicle group, **vitC** group, prodrug group, and the combination group. Each was given IP doses each day (5 d per week) for 10 weeks. For the combination group, **vitC** IP injection was given 1 h prior to the prodrug IP injection. **vitC** was dissolved in DI water and pH adjusted to 7.0 with NaOH. The prodrug was formulated in a mixture of DMSO, poly(ethylene glycol) (PEG) 400, and phosphate-buffered saline (PBS) (volume ratio 2:19:19). The volume of injection for both compounds was 100 µL at a concentration of 3.0 mg/kg of the prodrug and 500 mg/kg of **vitC**. Mice were weekly weighed, and tumor sizes were measured using electronic calipers every 7 d. The tumor volume was calculated as follows:

$$V = (L\,x\,W^2)/2$$

At the end of the study period, all tumors, hearts, lungs, livers, kidneys, brains, and spleen were harvested, weighed, and stored in -80 °C for further analysis.

2.14. Hematoxylin and eosin (H&E) Staining

For histological morphometry and apoptosis analysis, tumor, and major organs, including heart, liver, kidney, lung, spleen, and brain were fixed with 10% formalin, later embedded in paraffin and cut into 5-µm-thick sections and stained with hematoxylin and eosin. Stained slides were Imaged using Hamamatsu WSI imager and analyzed using NDP.view2 software.

2.15. In Vivo Optical Imaging

Metabolic Activity: To assess tumor metabolic activity, one mouse from each treatment group (Vehicle,

vitC, **FAN-NM-CH$_3$**, and Combination) was selected at week 8 of the treatment. A 100 nmol IRDye 800CW 2-DG Optical Probe (LI-COR: 926-08946), with excitation/emission wavelengths of 770 nm/790 nm, was reconstituted in 2 mL of sterile 1X PBS to achieve a final concentration of 0.05 nmol/μL. 100 μL (5 nmol) of this stock solution was administered intravenously via the tail vein. 24 h after injection, the mice were euthanized and imaged for tumor metabolic activity using an *in vivo* imaging instrument. The probe signal was quantified using ImageJ software. Note that the probe is processed through the liver, the major site of glycolysis, and excreted through the kidneys and bladder, causing increased background when imaging these regions. *ROS Detection:* To investigate ROS levels at the tumor site, 4 mice with similar tumor size were left untreated for five weeks after the implantation of cancer cells, so the tumor can grow to a suitable size. During week 6 and 7, these four mice received similar treatment as the efficacy study by IP injection of Vehicle, **vitC**, **FAN-NM-CH$_3$**, and Combination. At the end of week 7, 1 mg of the ROS Brite 700 probe (ATT Bioquest: 16004), with excitation/emission wavelengths of 680 nm/700 nm, was reconstituted in 2 mL of sterile 1X PBS to achieve a final concentration of 0.5 μg/μL. 100 μL (50 μg) of this stock was administered intratumorally to each mouse under anesthesia with isoflurane 1 hour after their daily treatments. Mice were euthanized after 4 hours post-probe administration and imaged using an Odyssey Sa imager to determine relative ROS levels in different groups. The ROS signal was quantified using ImageJ software.

3. Results

*3.1. The combination of **vitC** and **FAN-NM-CH$_3$** results in potent and selective killing of cancer cells in vitro*

To explore the potential of combining prooxidants with ROS-responsive prodrugs, we evaluated the cytotoxicity of various prooxidants in cancer and normal cells and studied their effects on cancer cell killing in combination with ROS-responsive prodrug **FAN-NM-CH$_3$** (Fig. 1). Triple-negative breast cancer (TNBC) MDA-MB-468 cells and MCF 10A normal cells were selected for initial studies (Fig. 2, A to C). Among the prooxidants tested, including piperlongumine, β-lapachone, vitamin E, arsenic trioxide, propyl gallate, quercetin, and EGCG,(*7*) **vitC** demonstrated the highest safety profile and selectivity toward cancer cells, as indicated by its high IC_{50} values in both cancer and normal cells (Fig. 2A and fig. S1, A to E). At its maximum safe dose (MAXSD), **vitC** significantly enhanced the anticancer activity and selectivity of **FAN-NM-CH$_3$**, achieving a selectivity index (SI) of 73 (defined as the ratio of IC_{50} values in normal cells to those in cancer cells) (Fig. 2, B and C). For instance, in TNBC cells, 1 mM **vitC** reduced the IC_{50} of **FAN-NM-CH$_3$** from 3 μM to 0.5 μM, while in normal cells, it only marginally lowered the IC_{50} from 48 μM to 36 μM (Fig. 2, B and F). Similar results were observed with other cancer and normal cell lines (Fig. 2D and fig. S2, A to D). These data suggest that **vitC** and ROS-responsive prodrug **FAN-NM-CH$_3$** act synergistically in cancer cells but not in normal cells, as indicated by combination index (CI) values calculated using the Chou and Talalay method (synergism: CI < 1.0) (Fig. 2D).(*27*) The combination yielded CI values of 0.58–0.87 across various cancer cell lines but showed no synergism in two normal cell lines (CI ~1), underscoring the universality and specificity of this strategy (Fig. 2, E and F, and Table S3). Collectively, these data demonstrate that **vitC** is an ideal prooxidant to be used in combination with ROS-responsive prodrugs to achieve potent and selective tumor killing.

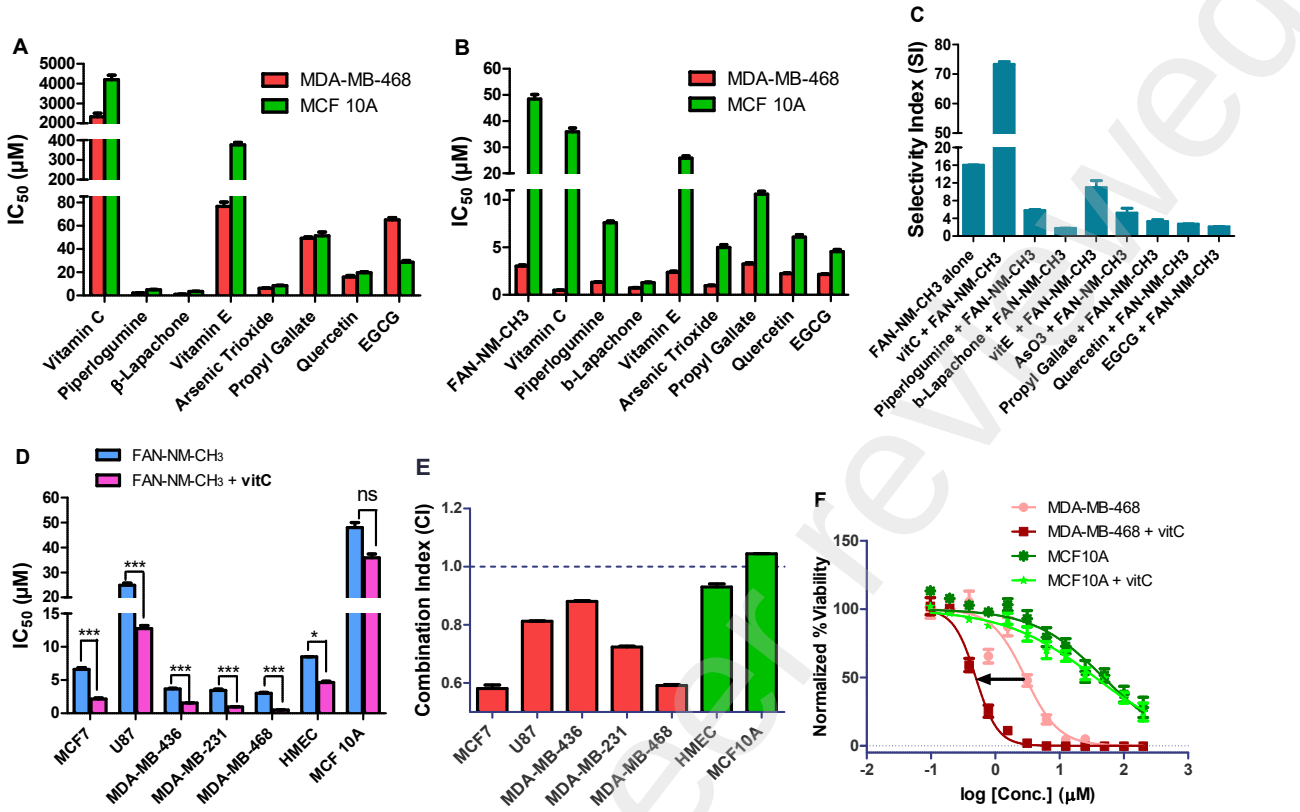

Fig. 1. **The cytotoxicity and selectivity of various prooxidants, FAN-NM-CH$_3$ alone or combination therapy on various cancer and normal cells** (**A-C**: data obtained with MDA-MB-468 cancer cells and MCF 10A normal cells; D-F: data obtained with various cancer and normal cell lines). (**A**) The IC_{50} values of prooxidants alone; (**B**) The IC50 values of **FAN-NM-CH$_3$** alone or in combination with MAXSD of prooxidants; (**C**) Selectivity Index (SI) of **FAN-NM-CH$_3$** alone or in combination with prooxidants; (**D**) The effect of MAXSD **vitC** on IC_{50} values of **FAN-NM-CH$_3$** in various tumor and normal cell lines; (**E**) Combination Index of combination therapy for different tumor and normal cell lines; (**F**) A representative example of IC_{50} curve of **FAN-NM-CH$_3$** with or without **vitC** in cancer (MDA-MB-468) and normal (MCF 10A) cells. [the data represent three independent experiments performed in triplicate (n = 3)].

The synergistic effect of **vitC** and **FAN-NM-CH$_3$** was further validated using SynergyFinder 3.0, employing multi-dose assays to minimize false positives.(*29*) A 5 x 5 concentration matrix was designed (0-5 μM **FAN-NM-CH$_3$** and 0-4.0 mM **vitC**) (Fig. 3 and fig. S3). Cell viability data analyzed using SynergyFinder 3.0 (Bliss Independence model) revealed high synergy scores (6.75–24.459) in cancer cells, with large synergy regions (red) on 2D and 3D landscapes (Fig. 3A, and fig. S3). No antagonistic interactions were observed in cancer cells, whereas normal cells (MCF 10A) displayed a large antagonistic region (green) (Fig. 3B). Among cancer cell lines, MDA-MB-468 (synergy score: 24.459) and MCF7 (17.078) were more sensitive to the combination than glioblastoma U87 cells (6.75), reflecting glioblastoma's known resistance to chemotherapeutic agents.(*30*) Nevertheless, **vitC** sensitized glioblastoma cells to **FAN-NM-CH$_3$** while sparing normal cells. These findings highlight the robustness of this combination strategy in selectively targeting cancer cells.

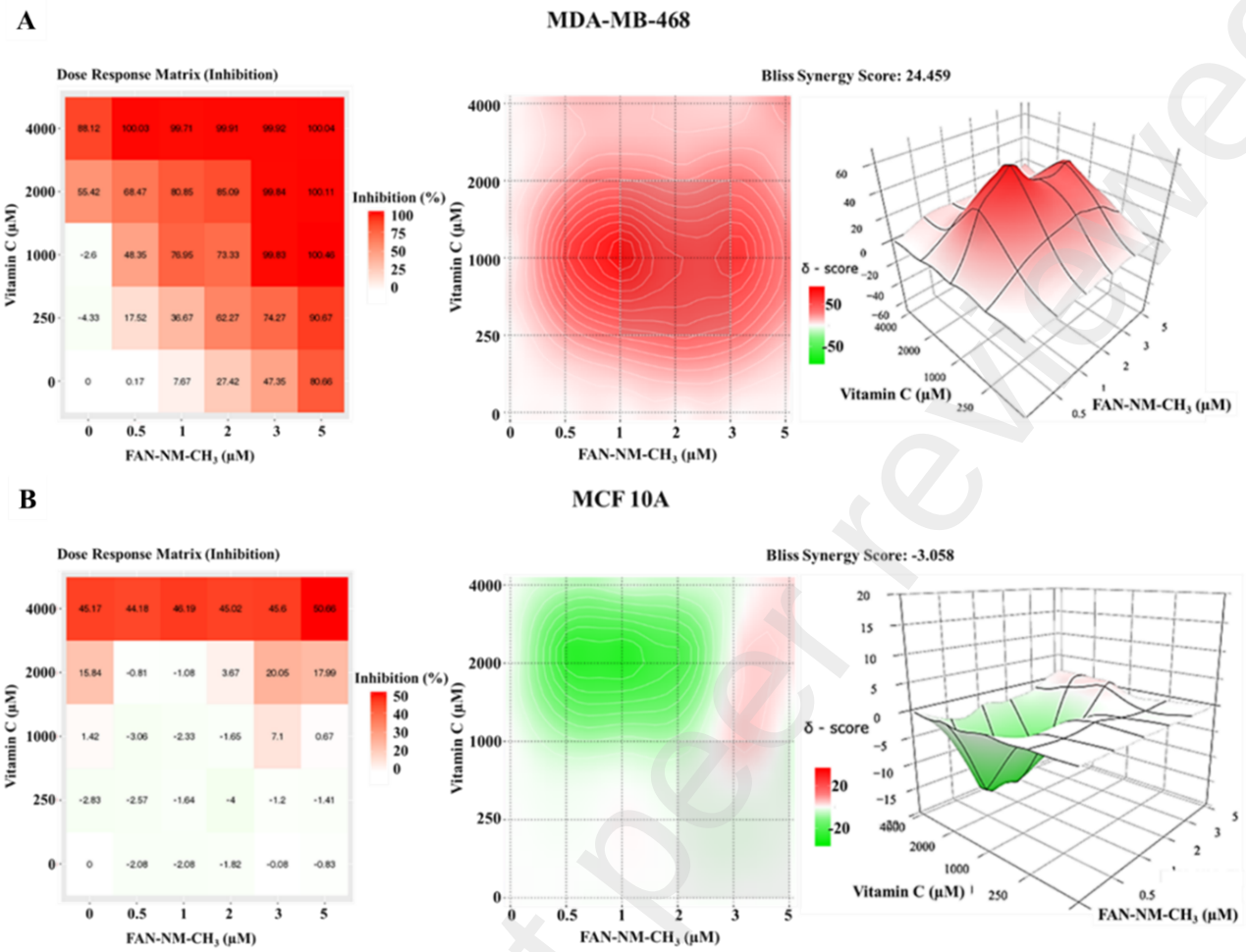

Fig. 3. **The drug synergy test for vitC and FAN-NM-CH$_3$ by SynergyFinder 3.0 with Dose Response Matrix (left), the drug interaction 2D (middle) and 3D (right) landscapes based on the Bliss mode**l. The synergy score is shown by Red (> 0) and Green (< 0). A synergy score of < -10 means the interaction is likely to be antagonistic, between -10 to 10 means it's likely to be additive, and > 10 means it is likely to be synergistic. Tests were performed on data generated from cytotoxicity studies on (**A**) MDA-MB-468 and (**B**) MCF 10A cells when treated for 48 h and data was normalized with their respective untreated controls. All cytotoxicity data used for the synergy score represents 3 independent replicate experiments, mean ± SD (n = 3).

*3.2. The synergy of **vitC** and **FAN-NM-CH$_3$** in tumor cell killing is driven by **vitC**-induced H$_2$O$_2$ coupled with cancer cells' limited catalase activity.*

To elucidate the mechanism underlying the synergistic anticancer effects of **vitC** and **FAN-NM-CH$_3$**, chlorambucil (**Chlor**), a non-H_2O_2-activated DNA alkylating agent, was tested alongside **vitC** (fig. S2, C to F). The combination of **Chlor** and **vitC** showed an antagonistic effect (CI = 1.38, DRI = 1) (fig. S2F), highlighting the necessity of the H_2O_2-responsive boronic acid group in **FAN-NM-CH$_3$** for selective prodrug activation. As **FAN-NM-CH$_3$** is activated by H_2O_2, we assessed H_2O_2 level and catalase activity a key enzyme that breaks down H_2O_2 to water and oxygen. MDA-MB-468, MCF7, U87, and MCF 10A cells were selected as representative models for TNBC, HR+ breast cancer, glioblastoma, and non-tumorigenic breast epithelial cells, respectively. Cancer cells (MDA-MB-468, MCF7, U87) displayed higher baseline H_2O_2 levels (Fig. 4A) and lower catalase activity compared to normal cells (MCF10A) (Fig. 4B and fig. S4). **VitC** further increased H_2O_2 levels selectively in cancer cells (Fig. 4C, and fig. S5 and S6). Based on these findings, we propose that **vitC**-induced H_2O_2 generation drives the synergistic

anticancer effects of **vitC** and **FAN-NM-CH$_3$** via selective prodrug activation in cancer cells, while the higher catalase activity in normal cells mitigates H_2O_2 accumulation, thereby reducing prodrug activation and cytotoxicity in normal cells.

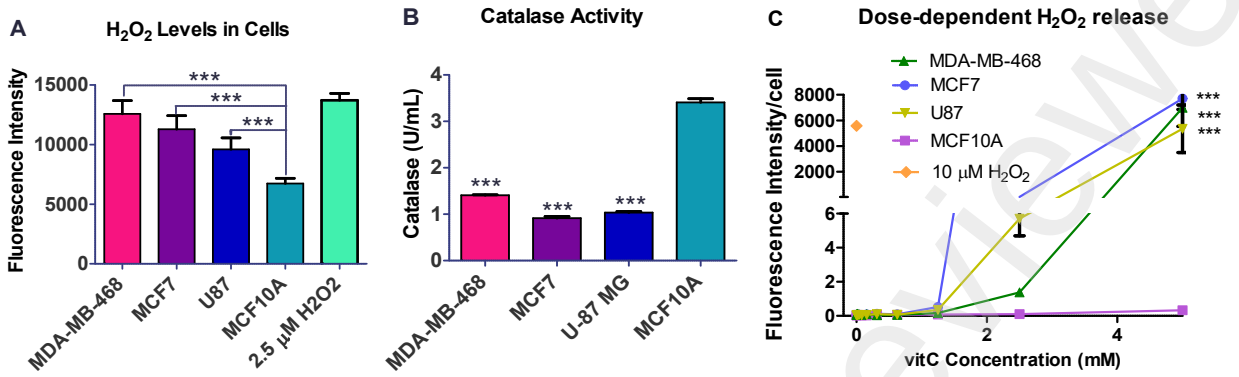

Fig. 4. H_2O_2 level in different cell lines and catalase activity. (**A**) Extracellular H_2O_2 levels in various cell lines (n = 3) (H_2O_2 level was measured by Amplex Red in culture medium immediately after removing the cells); (**B**) Catalase activity in different cell lines (n = 3); (**C**) Dose-dependent H_2O_2 generation induced by **vitC**. The significance was determined by one-way ANOVA followed by Dunnett to compare all columns (n = 4), (*) $P < 0.05$, (***) $p < 0.0001$ vs normal cell MCF10A.

To further validate the role of H_2O_2 in the synergistic anticancer effects, we investigated the impact of catalase on cell viability and H_2O_2 production. Cells were treated with **vitC** alone, **FAN-NM-CH$_3$** alone, or their combination, with or without catalase supplementation (Fig. 5 and figs. S7 to S10). A combination of safe doses of **vitC** and **FAN-NM-CH$_3$** lead to significant cancer cell death (~40%-80%), while catalase addition markedly diminished the combined cytotoxicity of **vitC** and **FAN-NM-CH$_3$** by quenching H_2O_2 and preventing **FAN-NM-CH$_3$** activation (Fig. 5, A and B, and fig. S7 and S8). This phenomenon was also observed with other dose ranges (fig. S11 to S15). **FAN-NM-CH$_3$** alone did not induce H_2O_2 production; however its combination with **vitC** caused significant H_2O_2 elevation in cancer cells (e.g., ~5-fold in MDA-MB-468) without affecting normal cells. This increase strongly correlated with the combination's selective killing of cancer cells (Fig. 5, B and C). Notably, MDA-MB-468 cells exhibited the highest H_2O_2 levels, corresponding to the greatest synergistic anticancer effect of the combination therapy. These findings underscore the essential role of **vitC**-induced H_2O_2 in the activation of **FAN-NM-CH$_3$** and the resultant cytotoxic effects on cancer cells.

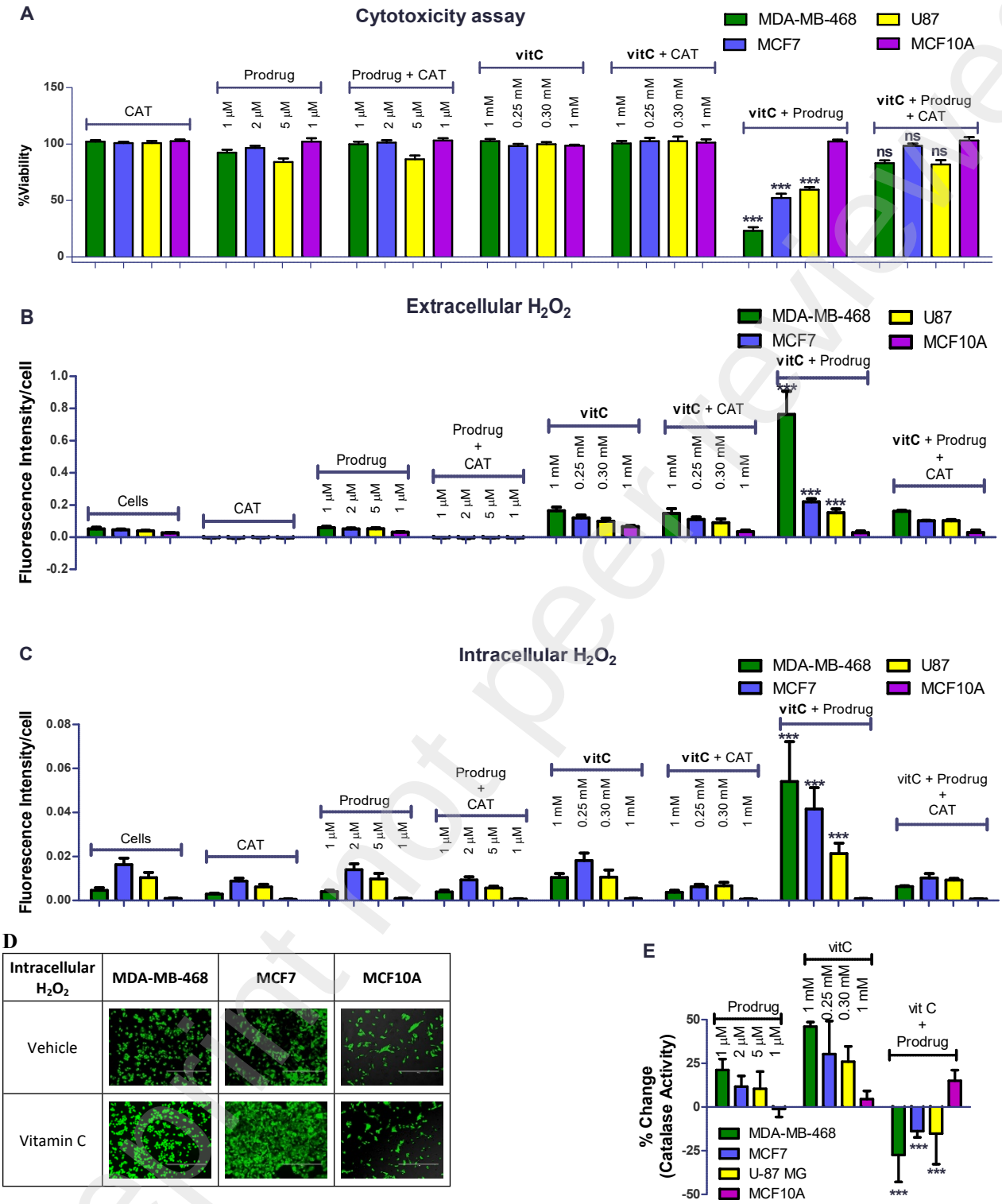

Fig. 5. Correlation between cell viability and H_2O_2 level as well as catalase activity. (**A**) Cell viability upon treatment under different conditions; (**B**) Extracellular H_2O_2 levels measured by Amplex Red Hydrogen Peroxide/Peroxidase Assay (Invitrogen: A22188); (**C**) Intracellular H_2O_2 levels assessed by Hydrogen Peroxide Assay Kit (abcam: ab138874) that uses cell-permeable AbGreen indicator to quantify H_2O_2 in live cells; (**D**) Representative images of intracellular H_2O_2 levels measured by Hydrogen Peroxide Assay Kit (abcam: ab138874) (Scalebar = 400 µm); (**E**) The change of catalase activity in different cell lines treated

under different conditions (n = 3). MDA-MB-468, MCF7, U87, and MCF 10A cells were treated with MAXSD of **FAN-NM-CH_3** (1 µM, 2 µM, and 5 µM), or **vitC** (1 mM, 0.25 mM, 0.30 mM and 1 mM), or combination of **FAN-NM-CH_3** and **vitC** at 37 °C for 48 hours. The significance was determined by one-way ANOVA followed by Dunnett to compare all columns (n = 4), (*) $P < 0.05$, (***) $p < 0.0001$ vs normal cell MCF10A.

To elucidate the mechanism for selective H_2O_2 intensification in cancer cells treated with **vitC** and **FAN-NM-CH_3**, we evaluated catalase activity across various treatments. Cancer cells treated with **vitC** or **FAN-NM-CH_3** alone showed increased catalase activity (10%-20% increase for **FAN-NM-CH_3** and 26%-46% for **vitC**) (Fig. 5E). However, the combination treatment led to a 14%-27% decrease in catalase activity, resulting in sustained H_2O_2 accumulation (2-7 fold increases) (Fig. 5, B and C). These data indicate that while cancer cells adapt to mild oxidative stress from individual agents by upregulating catalase activity, the combination therapy overwhelms their antioxidative defenses, leading to decreased catalase activity and enhanced H_2O_2 accumulation. In contrast, normal cells maintain high catalase activity irrespective of treatment, effectively neutralizing H_2O_2 and preventing cytotoxicity (Fig. 4B and 5E).

*3.3. The combination of **vitC** and **FAN-NM-CH_3** exacerbates DNA damage and cell apoptosis in cancer cells*

We hypothesize that **vitC**-induced H_2O_2 accumulation activates the prodrugs, releasing alkylating intermediates that induce DNA damage and drive cell death. This was evaluated using an alkaline comet assay in MDA-MB-468, MCF7, U87, and MCF10A cells. DNA damage, indicated by longer comet tails, was observed in cancer cells treated with the combination of **vitC** and **FAN-NM-CH_3** but not with individual agents or in normal cells (Fig. 6A). Quantification of the comet tail, tail moment, and tail olive moment by TriTek CometScore Software revealed the extent of DNA damage, with MDA-MB-468 (~75%) > MCF7 (~57%) > U87 (~34%) > MCF10A (~5%) (Fig. 6, B and C, fig. S16, and Table S5 and S6). This trend aligned with the synergistic cytotoxicity observed for the combination therapy. DNA damage, if unrepaired, triggers apoptosis. Annexin V/PI/DAPI staining that identifies apoptotic cells, confirmed that **vitC** and FAN-NM-CH_3 significantly increased apoptotic cell populations, particularly in breast cancer cells, while sparing normal cells (Fig. 6, D to).

A

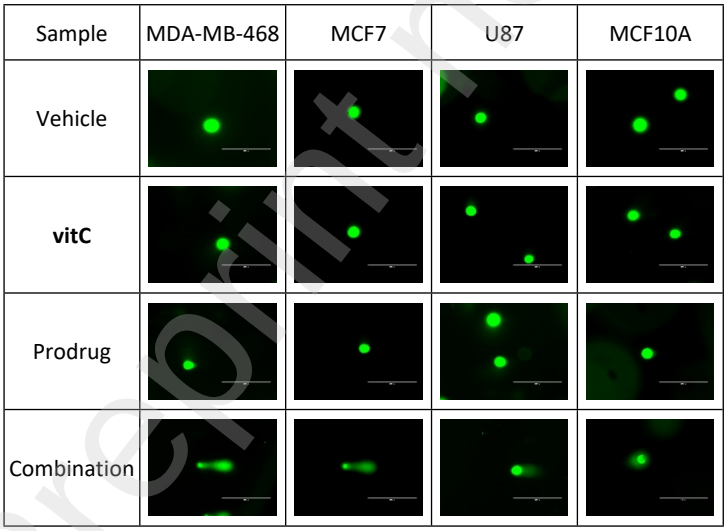

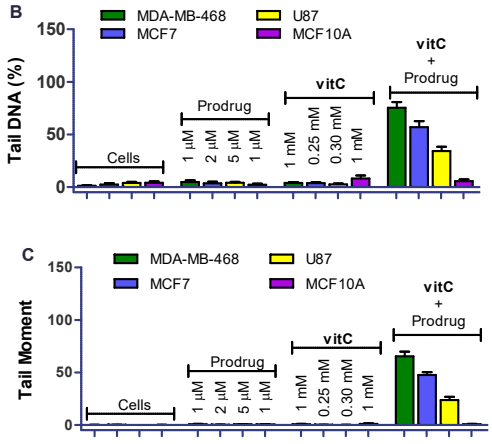

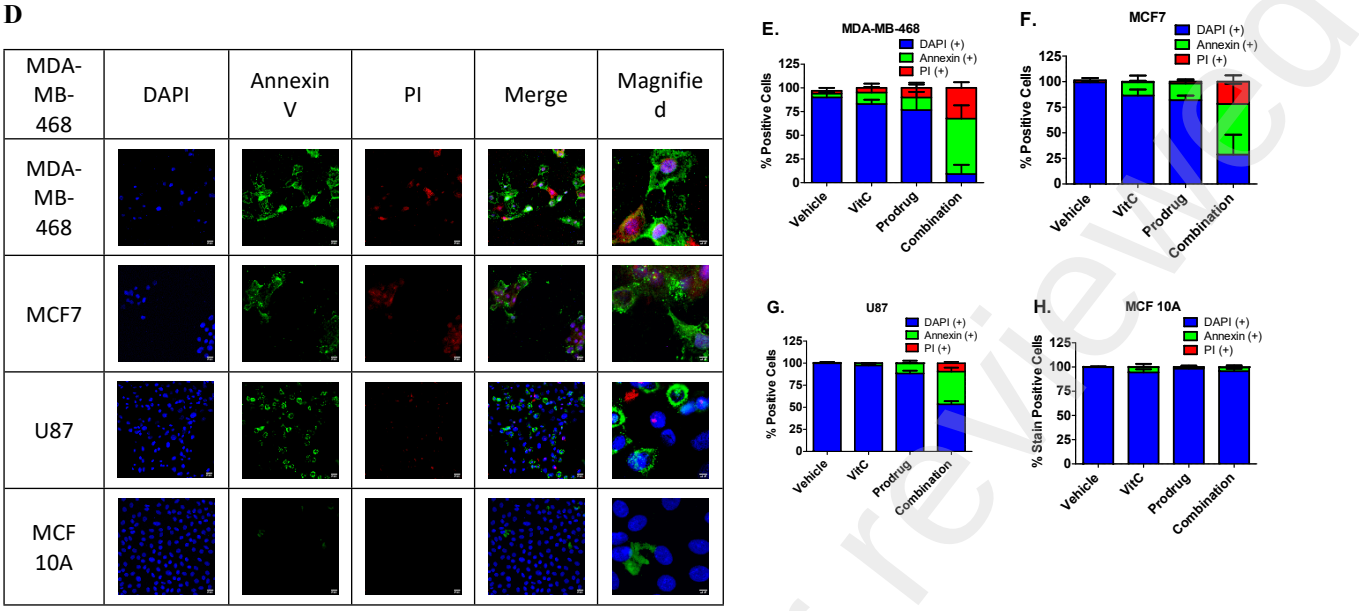

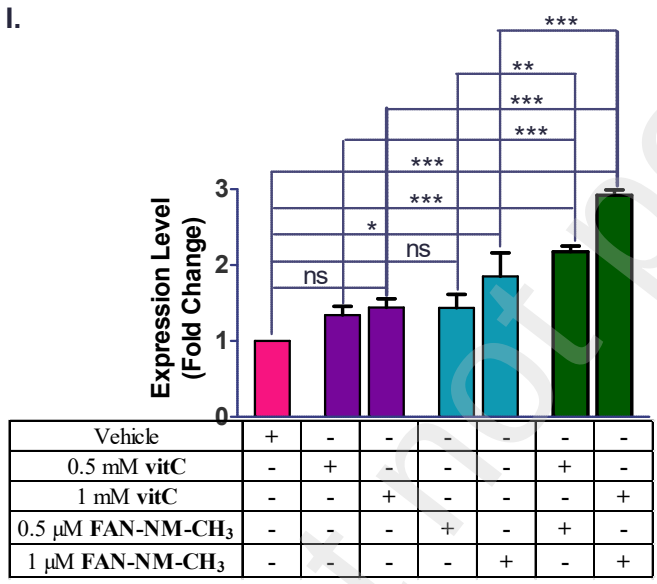

Fig. 6. A combination of safe doses of vitC and FAN-NM-CH_3 leads to DNA damage and p53 upregulation, triggering cancer cell apoptosis. (**A-C**) The alkaline comet assay analysis of MDA-MB-468, MCF7, U87, and MCF 10A cells after treatment with vehicle, **vitC**, **FAN-NM-CH_3**, and the combination: (**A**) Comet Images taken with EVOS Digital Inverted Microscope at 20X magnification; (**B**) Quantification of % DNA in the tail of the comets; (**C**) Quantification of Tail moment (Images were analyzed by TriTek CometScore Software). Each data point represents 3 independent replicate experiments, and the data are presented as the mean ± SD (n = 3). (**D-H**) Determination of cell death pathway by Annexin V/PI/DAPI staining using fluorescence confocal microscopy: (**D**) The representative images of Annexin V/PI/DAPI staining of cells treated with combination (The scale bar represents 10 µm for the overall image and 2.5 µm for the magnified section); (**E-H**) quantification of stain positive cell population (%) using software ImageJ, n = 3. Images represent at least 5 fields observed in 3 different preparations after 48 h of treatment. **(I)** p53 mRNA expression level (n = 3) of MDA-MB-468 cells treated with **vitC**, **FAN-NM-CH_3**, or combination. Data was normalized with relative GAPDH mRNA levels and fold change calculated with $2^{-\Delta\Delta Ct}$ method of Lovak and Schmittgen. The significance was determined by one-way ANOVA followed by Dunnett to compare all columns (n = 7), (*) $P < 0.05$, (***) $p < 0.0001$ vs vehicle.

DNA alkylating agents, such as chlorambucil, are reported to induce cell apoptosis via upregulation of the p53 gene, a key regulator of apoptosis.(*31*) To understand the combination therapy's effect on p53 expression, we quantified p53 mRNA levels in MDA-MB-468 cells. Low-dose **vitC** or **FAN-NM-CH_3** slightly increased p53 expression (~0.3-fold), while higher **FAN-NM-CH_3** doses induced a ~0.9-fold increase. Combination of safe doses of **vitC** (0.5 mM-1.0 mM) and **FAN-NM-CH_3** (0.5-1.0 µM) resulted in significant p53 upregulation (1.2- to 1.9-fold, depending on doses) (Fig. 6I). These results suggest that

slightly increased H_2O_2 levels induced by **vitC** alone has a minimum effect on p53 expression, whereas H_2O_2-mediated **FAN-NM-CH$_3$** activation drives increased DNA damage and p53 upregulation, leading to cancer cell apoptosis.

3.4. The combination of vitC and FAN-NM-CH$_3$ leads to regression of established tumors in mice without adverse effects

The efficacy and selectivity of the combination of **vitC** and **FAN-NM-CH$_3$** was further evaluated in vivo with xenograft mice model. Initially, we used CD-1 mice to determine the safe doses of combination therapy (fig. S17 to S20). No apparent signs of toxicity were observed with a combination of 5.0 mg or 10 mg/kg of **FAN-NM-CH$_3$** with **vitC** at doses of 0.5 - 3.0 g (fig. S17C to S17E). Mice treated with combination showed weight gains comparable to controls. Monitoring mouse health and welfare with a Mouse Intervention Scoring System (MISS) adapted from Koch et al. and Paster et al.,(*32, 33*) suggested that all mice treated with combination showed normal behavior with a terminal score >10 (fig. S17, G and H, and SI Table S8). However, 20 mg/kg dose of **FAN-NM-CH$_3$** exhibited significant weight loss when combined with **vitC** at doses of 500 - 1000 mg/kg (fig. S17F). Therefore, for the *in vivo* efficacy study, a low-dose combination of **FAN-NM-CH$_3$** (3 mg/kg) and **vitC** (500 mg/kg) was selected to evaluate synergistic effects while minimizing the influence of single-agent toxicity.

Athymic nude mice xenografted with human tumor cell lines were used to evaluate the efficacy and selectivity of the combination treatment (Fig. 7). MDA-MB-468 breast cancer cells were implanted subcutaneously in nude mice, resulting in tumor formation within one week (Fig. 7A). Mice were divided into four groups (n=5/group): vehicle, **vitC** (500 mg/kg), **FAN-NM-CH$_3$** (3 mg/kg), and a combination of **vitC** (500 mg/kg) and **FAN-NM-CH$_3$** (3 mg/kg). Treatments were administered IP for five days per week over ten weeks (Fig. 7 and fig. S21 to S25). For the combination group, **vitC** was injected one hour before **FAN-NM-CH$_3$** administration (Fig. 7A). Tumor size, body weight,

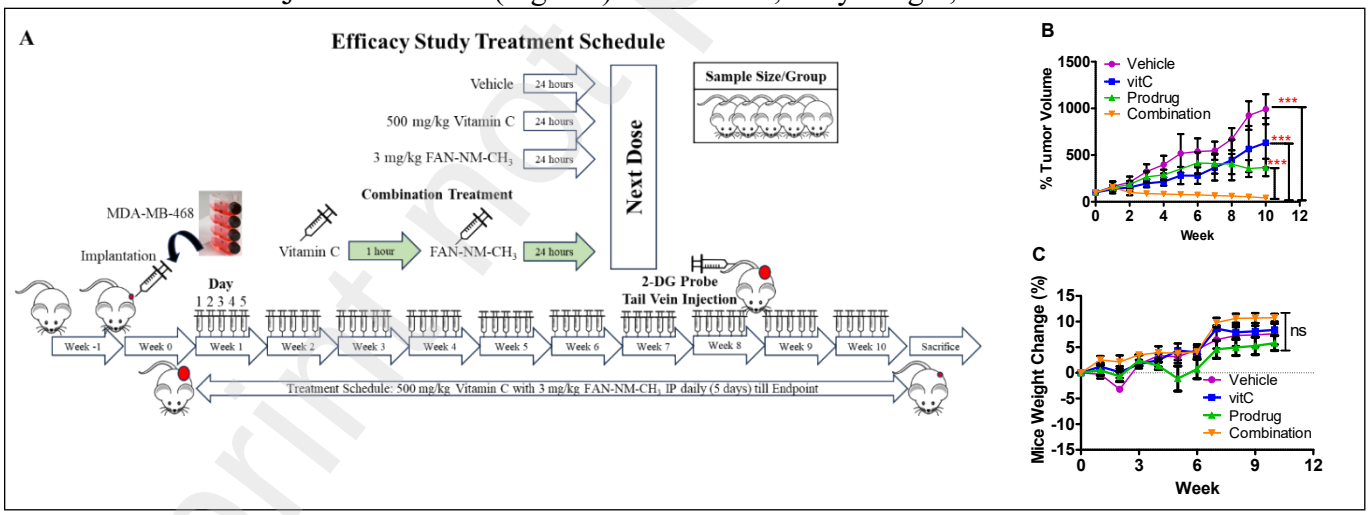

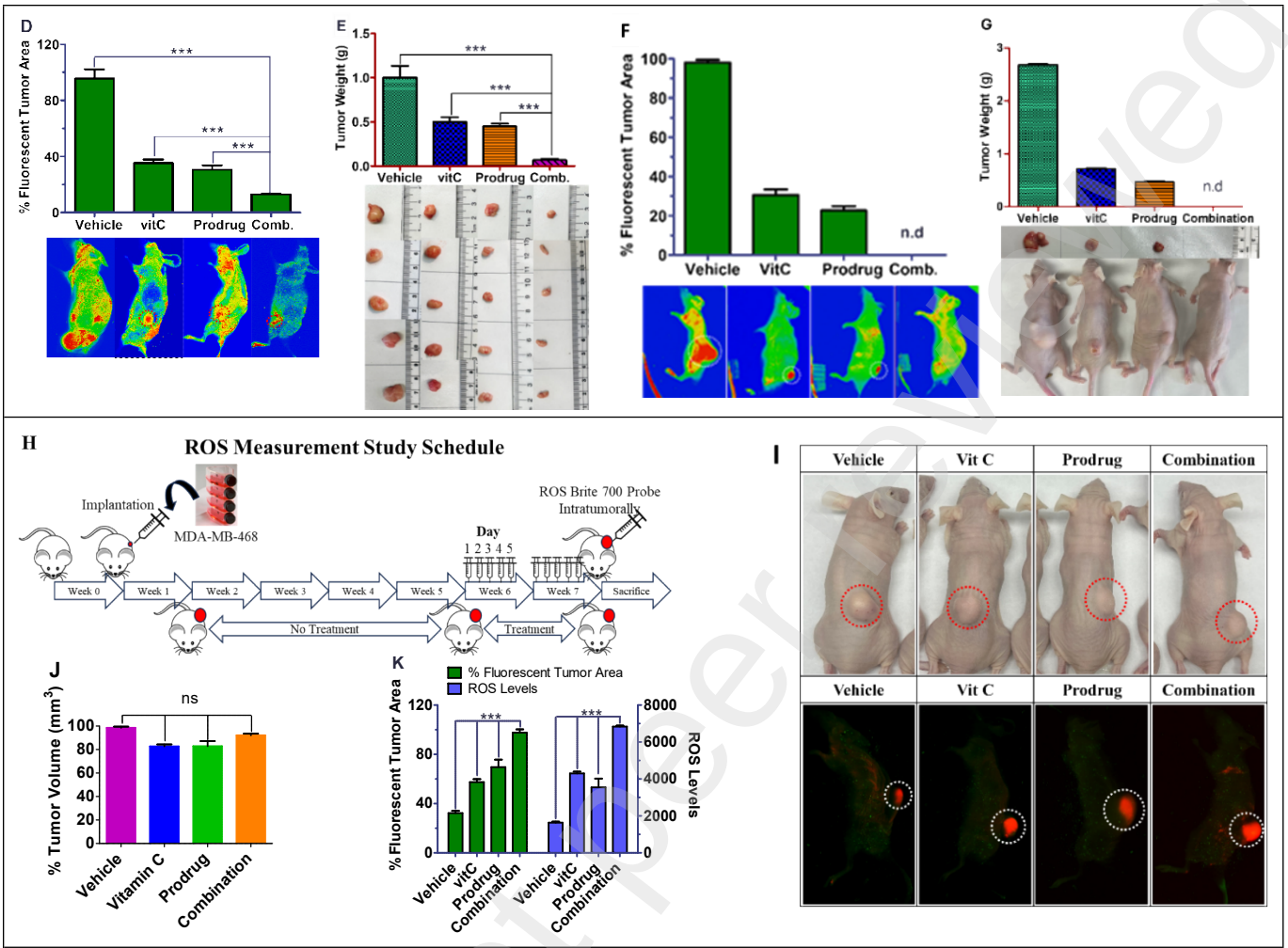

Fig. 7. In vivo antitumor efficacy and safety. (A) Scheme of the treatment timeline for the in vivo efficacy study and 2DG probe administration; (B) Tumor volumes measured by caliper; (C) Time-dependent mice weight change %; (D) Tumor regression indicated by the whole mice image and quantification of the tumor fluorescent area using ImageJ software; (E) Tumor weights at the end of 10-week treatment and photos of the harvested tumors; (F and G) Tumor sizes after 23 weeks including10-week treatment and 13-week post-treatment observation: (F) the whole mice imaging and quantification of the tumor fluorescent area using ImageJ software (n.d.: not detected); (G) tumor weight, appearance, and photos of the harvested tumors; (H-K): Evaluation of ROS level in mouse tumor: (H) ROS measurement study schedule (mice received ROS Brite 700 probe intratumorally five weeks after inoculation with MDA-MB-468 cells); (I) Mice appearance and fluorescent images; (J) Tumor volumes measured by caliper; (K) The fluorescent tumor area (%) and weighted fluorescent index. Fluorescent tumor area (%) and mean fluorescence intensity were quantified by ImageJ software. Weighted Fluorescence Index is defined as the product of % Fluorescent Tumor Area and the corresponding Mean Fluorescence Intensity. Each data point represents 3 independent replicate experiments, and the data are presented as the mean ± SD (n = 3). The significance was determined by one-way ANOVA followed by Dunnett to compare all columns (n = 4), (*) $P < 0.05$, (***) $p < 0.0001$ vs combination-treated mice.

health, and behavior were monitored weekly. Tumor volumes were measured weekly using calipers and the whole mice imaging conducted at week 8. The combination treatment not only inhibited tumor growth but also induced significant tumor shrinkage (Fig. 7B, and fig. S21). In comparison with **vitC** or **FAN-NM-CH$_3$** alone, the combination of the two greatly enhanced their *in vivo* efficacy without causing side effects (Fig. 7, B and C, and fig. S22). Tumors in combination-treated mice decreased to approximately 80% of their initial size after three weeks and 40% after ten weeks (Fig. 7B). In contrast, vehicle-treated mice experienced a 1000% increase in tumor size. While **vitC** or **FAN-NM-CH$_3$** alone slightly inhibited tumor growth, neither caused tumor shrinkage (Fig. 7B). By week 10, the average tumor volume in the

combination group (42 ± 7.5 mm³) was only 4% of the control group (991 ± 226.4 mm³), compared to 64% and 37% for **vitC** (631 ± 458.9 mm³) and **FAN-NM-CH$_3$** (367 ± 185.4 mm³), respectively. The tumor growth inhibition rate [IR (%) = [1 − (mean volume of treated tumors)/(mean volume of control tumors)] × 100] was 96% for the combination, 63% for FAN-NM-CH$_3$ alone, and 36% for **vitC** alone.

Whole mouse fluorescence imaging confirmed significant tumor regression in the combination group (Fig. 7D). At week-8, the mice were injected with infrared dye 800-conjugated 2-deoxy-d-glucose (2-DG) via tail-vein and imaged in a LI-COR Odyssey infrared scanner (Fig. 7A). Tumors, due to heightened metabolic activity, produced a stronger fluorescent signal than the rest of the body. The combination-treated mouse showed the smallest fluorescent tumor area (13% relative to the vehicle mouse). Tumors excised at week 11 further confirmed these findings. Average tumor weights were significantly lower in the combination group (67.5 ± 26.8 mg) compared to **vitC** (500.0 ± 91.6 mg), **FAN-NM-CH$_3$** (450.0 ± 52.4 mg), and vehicle groups (1003.3 ± 185.2 mg) (Fig. 7E). These results demonstrate that the combination of **vitC** and **FAN-NM-CH$_3$** leads to regression of established tumors in mice.

To evaluate long-term effects, in a separate experiment, mice were monitored for 13 weeks after the 10-week treatment. Combination-treated mice exhibited no delayed adverse effects or tumor recurrence, with complete tumor regression observed (Fig. 7, F and G, and figs. S23, A to D). In contrast, tumors in vehicle, **vitC**, and **FAN-NM-CH$_3$** groups grew significantly during this period, with control tumors reaching 2300% of their original size, 800% for **vitC** group, and 600% for **FAN-NM-CH$_3$** group (fig. S23, C and D). Whole mice imaging with a 2-DG probe further confirmed our observations (Fig. 7F). No detectable fluorescence (indicating a tumorous area) was found in combination-treated mice, while tumor regions with strong fluorescent signals were detected in control mice, **vitC**-treated mice, and **prodrug**-treated mice. Tumor weights were 2.68 g for control mouse, 0.71 g for **vitC**-treated mouse, and 0.47 g for prodrug-treated mouse (Fig. 7G).

The four groups of nude mice from the *in vivo* efficacy study were monitored for symptoms of toxicity, including body weight changes, appetite loss, lethargy, treatment-related mortality, and organ health (Fig. 7C, and figs. S22, S24, and S25). Mice treated with **vitC** (500 mg/kg), **FAN-NM-CH$_3$** (3 mg/kg), or their combination exhibited no signs of toxicity. In fact, all groups showed weight gains during the 10-week study and 13-week post-treatment observation (Fig. 7C and fig. S22). Weekly scoring confirmed overall terminal scores >10, with no evidence of organ dysfunction (figs. S23 and S24). Histological analysis of heart, liver, spleen, kidney, lung, and brain tissues from treated mice revealed no significant pathological changes or toxicity (fig. S25 and Table S11). All organ architectures remained intact, with no inflammation, fibrosis, or cellular damage observed. These findings indicate that the combination treatment is well-tolerated by mice without adverse effects on these major organs. Together, the *in vivo* investigation demonstrated that a combination of **vitC** with ROS-responsive prodrugs leads to potent and selective tumor killing without affecting normal tissues in mice.

Cell culture studies have revealed that ROS levels play a crucial role in the synergistic anticancer efficacy and selectivity of the combination therapy involving **vitC** and **FAN-NM-CH$_3$**. To validate this finding in vivo, tumor ROS levels were measured using the ROS Brite 700 (RB 700) probe, which fluoresces upon ROS oxidation (Fig. 7H). The study was conducted five weeks after tumor cell inoculation, when all mice had reached a suitable tumor size (Fig. 7, I and J). To eliminate potential discrepancies due to tumor volume, the RB 700 probe was injected after two weeks of treatment, when all mice had similar tumor sizes. The tumor volume relative to the vehicle was 92% in combination-treated mice, and 83% in both prodrug and vitC-treated mice (Fig. 7J). In vivo fluorescence imaging on the Odyssey Sa imager indicated

that tumor cells were under oxidative stress in all mice (Fig. 7I). The ROS level, as indicated by the % fluorescent tumor area, followed the order: combination-treated mice > **FAN-NM-CH_3**-treated mice > **vitC**-treated mice > control mice (Fig. 7K). Tumors naturally produce ROS due to their high metabolic activity, but **vitC** and **FAN-NM-CH_3** further elevated oxidative stress, with the combination treatment showing the highest ROS levels, correlating with the highest antitumor effects. The Weighted Fluorescence Index (fluorescent tumor area × mean intensity) ranked as follows: combination (6833) > vitC (4303) > prodrug (3548) > vehicle (1634) (Fig. 7K). These results strongly suggest a correlation between elevated ROS levels and the enhanced *in vivo* anticancer efficacy of the **vitC** and **FAN-NM-CH_3** combination therapy.

4. Discussion and conclusion

Cancer cells are more susceptible than normal cells to disruptions in redox homeostasis.(*3, 5, 34*) The notion of exploiting this vulnerability to selectively target tumors, known as oxidative stress-based cancer therapy, has gained traction in recent decades.(*2-4, 6*) Numerous pro-oxidants have been identified for their ability to induce oxidative stress in cancer cells, showing promising results in certain cases.(*2-7*) However, challenges such as limited tumor selectivity and therapeutic durability often hinder their clinical application. In this study, we address these limitations by combining pro-oxidants with ROS-responsive prodrugs. This approach leverages pro-oxidants to amplify oxidative stress within tumors, enhancing the sensitivity of cancer cells to ROS-responsive prodrugs and achieving a synergistic anticancer effect.

Among various prooxidants, **vitC** emerges as a preferred candidate for combination with ROS-responsive prodrugs due to its superior safety profile for normal cells. The antitumor potential of **vitC** as a therapeutic agent is well-documented, with extensive research focused on high-dose **vitC** or combining **vitC** with standard chemotherapy or radiotherapy to enhance therapeutic outcomes (*35-40*). However, clinical results regarding the efficacy of high-dose **vitC**, either as a standalone treatment or in combination with other chemotherapeutic agents, remain inconsistent.(*37-40*). In this work, we discovered a novel application of **vitC** to potentiate the effects of ROS-responsive prodrugs. Numerous studies have demonstrated that non-toxic prodrugs with a H_2O_2-responsive boronate ester/boronic acid functional group can be selectively activated by ROS, releasing cytotoxic agents specifically in cancer cells with elevated ROS levels.(*14-23*) While ROS-activated prodrugs showed promise in improving tumor specificity and minimizing adverse side effects, challenges remain in developing effective targeted cancer therapies. These include tumor ROS heterogeneity, non-targeted drug delivery, insufficient activation, and limited therapeutic durability. For example, the H_2O_2 concentration in many cancer cells may be insufficient to trigger the targeted release of therapeutic agents. Our findings reveal that **vitC** enhances the efficacy of ROS-responsive prodrugs, providing the first evidence that certain pro-oxidants can be effectively combined with ROS-responsive prodrugs to overcome these limitations.

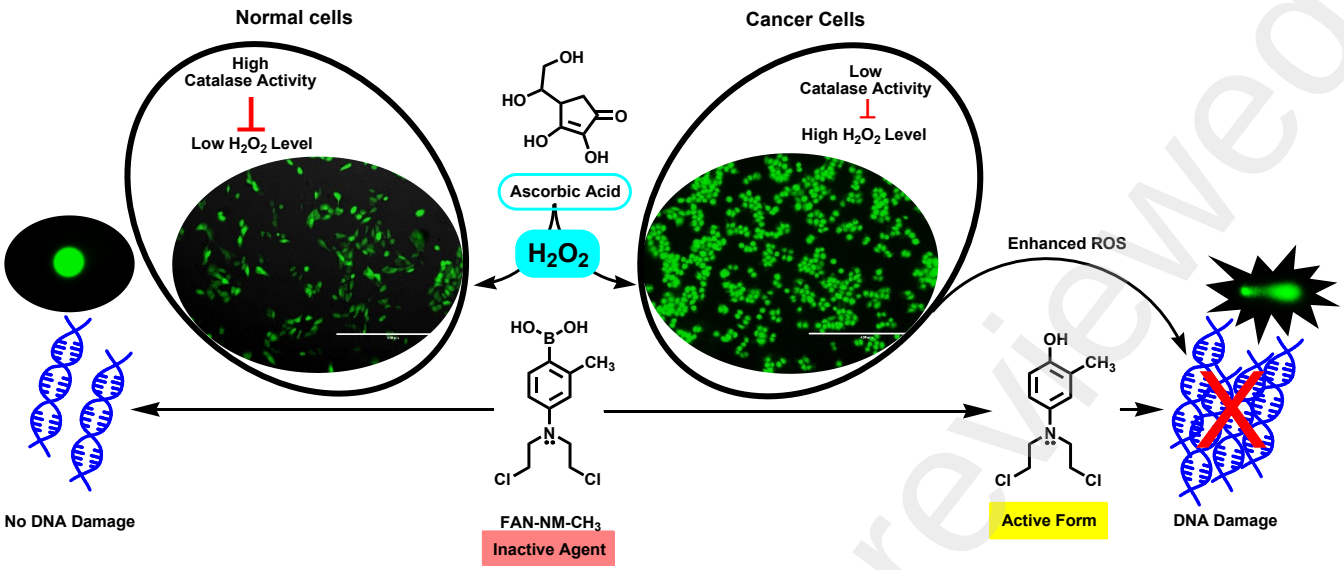

Fig. 8. Graphical representation of vitC-induced H_2O_2 generation that activates H_2O_2-responsive prodrug specifically in cancer cells leading to DNA damage and cell apoptosis.

VitC selectively induces H_2O_2 generation in cancer cells, triggering the activation of ROS-responsive prodrugs to release cytotoxic species (Fig. 8). This dual action not only causes DNA damage through prodrug activation but also elevates ROS levels, resulting in extensive cancer cell death via apoptosis. The selectivity of this combination treatment between cancer and normal cells is governed by catalase activity. Cancer cells, which inherently have low catalase activity, experience a further reduction in catalase upon treatment with the **vitC**/prodrug combination. This leads to substantial H_2O_2 accumulation, enhanced prodrug activation, and a robust and selective tumor-killing effect. In contrast, normal cells, characterized by high catalase activity, adapt to the oxidative stress induced by the treatment by further upregulating catalase, thereby protecting themselves from elevated ROS levels and prodrug activation. This differential response underpins the selective nature of the therapy and provides a strong basis for further exploration. *In vivo* study with xenograft mice provides further evidence on strong correlation between the *in vivo* synergistic anticancer effect of this combination therapy and elevated tumor ROS levels. Mice treated with a combination of **vitC** and the prodrug showed elevated tumor ROS levels in comparison with the mice treated with single agent. Meanwhile, the combination achieved complete tumor regression without recurrence, significantly outperforming single-agent treatments. Importantly, this approach not only delivers effective anticancer outcomes at low doses but also minimizes side effects and shows promise against aggressive cancers such as triple-negative breast cancer and glioblastoma.

Although we focused on **vitC** in this study, we postulate that the ROS-inducing component of our approach should not be restricted to small compound prooxidants but instead can be extended to a variety of biologics. We and others show that adoptive transfer of tumor-specific T cells, or infusion of immune checkpoint antibodies, can cause excessive ROS accumulation in cancer cells, contributing to tumor regression in multiple preclinical models(*41-45*). Rational combination of tumor redox-modulating agents and cancer immunotherapy is emerging as a promising treatment strategy(*46*). The potential combination of our ROS-responsive prodrugs with immunotherapies is currently under investigation.

In summary, our study establishes a novel way to unleash the antitumor potency of ROS-responsive prodrugs in a highly tumor-selective manner. This approach takes advantage the synergy between a ROS-inducing prooxidant and a ROS-responsive prodrug to mediate robust tumor killing. Our findings highlight the potential of this strategy in treating some challenging cancer types.

Statistical analysis

Data were analyzed using GraphPad Prism 5 (GraphPad Software, Sandiego, CA) and expressed as the mean ± SEM. A student t test was used to find the significance between 2 groups. Comparison of the multiple groups was done using one-way ANOVA analysis. P value of less than 0.05 was considered to be statistically significant. **Power analysis:** Groups of 5 mice are determined with GPower 3.1 based on the desire to show a significance level of 0.05 and the results of a pilot study.

Author contributions.

T.A., and X.P. designed research; T.A., T.N.F.P., A.K.P., H.G., J.P., D. L., J.A.R.J., and G.E.K. performed research; HF synthesized prodrug FAN-NM-CH3; X. P. supervised research; L.A.A., and A.R. contributed analytic tools; J.J., Y.C.C., and G. Z. analyzed data; T.A. and X.P. wrote the paper, and D. L. and G. Z. proofread and revised the paper.

Data and materials availability

All data needed to evaluate the conclusions in the paper are present in the paper and/or the Supplementary Materials.

Funding sources

This work was supported in part by the National Cancer Institute (1R15CA277656-01), UWM Research Foundation Bradley Catalyst Grant Program, UWM Discovery and Innovation Grant, and Great Milwaukee Foundation (Shaw Scientist Award). Alexis Kimberly Peterson was supported in part by UWM Senior Excellence in Research Awards. The undergraduates were also supported in part by UWM Support for Undergraduate Research Fellows (SURF) program.

Declaration of competing interest

The authors declare no competing interests.

Acknowledgments

We thank Prof. R. Kip Guy for helpful discussions and Dr. H. Li for critical reading of this manuscript. We also thank J. Nemke (Animal Resource Center, UW-Milwaukee) for providing advice on animal experiments and animal welfare.

References

1. G. Y. Liou, P. Storz, Reactive oxygen species in cancer. *Free Radic Res* **44**, 479-496 (2010).

2. C. Gorrini, I. S. Harris, T. W. Mak, Modulation of oxidative stress as an anticancer strategy. *Nat Rev Drug Discov* **12**, 931-947 (2013).
3. D. Trachootham, J. Alexandre, P. Huang, Targeting cancer cells by ROS-mediated mechanisms: a radical therapeutic approach? *Nat Rev Drug Discov* **8**, 579-591 (2009).
4. V. Nogueira, N. Hay, Molecular pathways: reactive oxygen species homeostasis in cancer cells and implications for cancer therapy. *Clin Cancer Res* **19**, 4309-4314 (2013).
5. P. T. Schumacker, Reactive oxygen species in cancer cells: live by the sword, die by the sword. *Cancer Cell* **10**, 175-176 (2006).
6. J. Wang, J. Yi, Cancer cell killing via ROS: to increase or decrease, that is the question. *Cancer Biol. Ther.* **7**, 1875-1884 (2008).
7. T. Ali *et al.*, Generation of Hydrogen Peroxide in Cancer Cells: Advancing Therapeutic Approaches for Cancer Treatment. *Cancers (Basel)* **16**, (2024).
8. Q. Chen *et al.*, Pharmacologic doses of ascorbate act as a prooxidant and decrease growth of aggressive tumor xenografts in mice. *Proc Natl Acad Sci U S A* **105**, 11105-11109 (2008).
9. Q. Chen *et al.*, Pharmacologic ascorbic acid concentrations selectively kill cancer cells: action as a pro-drug to deliver hydrogen peroxide to tissues. *Proc Natl Acad Sci U S A* **102**, 13604-13609 (2005).
10. Q. Chen *et al.*, Ascorbate in pharmacologic concentrations selectively generates ascorbate radical and hydrogen peroxide in extracellular fluid in vivo. *Proc Natl Acad Sci U S A* **104**, 8749-8754 (2007).
11. J. Yun *et al.*, Vitamin C selectively kills KRAS and BRAF mutant colorectal cancer cells by targeting GAPDH. *Science* **350**, 1391-1396 (2015).
12. J. Peiro Cadahia, V. Previtali, N. S. Troelsen, M. H. Clausen, Prodrug strategies for targeted therapy triggered by reactive oxygen species. *Medchemcomm* **10**, 1531-1549 (2019).
13. E. Saxon, X. Peng, Recent Advances in Hydrogen Peroxide Responsive Organoborons for Biological and Biomedical Applications. *Chembiochem* **23**, e202100366 (2022).
14. S. X. Huang *et al.*, Leinamycin E1 acting as an anticancer prodrug activated by reactive oxygen species. *P Natl Acad Sci USA* **112**, 8278-8283 (2015).
15. Y. Kuang, K. Balakrishnan, V. Gandhi, X. Peng, Hydrogen peroxide inducible DNA cross-linking agents: targeted anticancer prodrugs. *J Am Chem Soc* **133**, 19278-19281 (2011).
16. X. Peng, V. Gandhi, ROS-activated anticancer prodrugs: a new strategy for tumor-specific damage. *Ther Deliv* **3**, 823-833 (2012).
17. W. Chen *et al.*, Discovery and Optimization of Novel Hydrogen Peroxide Activated Aromatic Nitrogen Mustard Derivatives as Highly Potent Anticancer Agents. *J Med Chem* **61**, 9132-9145 (2018).
18. W. Chen *et al.*, Reactive oxygen species (ROS) inducible DNA cross-linking agents and their effect on cancer cells and normal lymphocytes. *J Med Chem* **57**, 4498-4510 (2014).
19. H. Hagen *et al.*, Aminoferrocene-based prodrugs activated by reactive oxygen species. *J Med Chem* **55**, 924-934 (2012).
20. M. Schikora *et al.*, Activity of aminoferrocene-based prodrugs against prostate cancer. *Bioorg. Med. Chem. Lett.* **25**, 3447-3450 (2015).
21. S. Daum *et al.*, Lysosome-Targeting Amplifiers of Reactive Oxygen Species as Anticancer Prodrugs. *Angew. Chem. Int. Ed. Engl.* **56**, 15545-15549 (2017).
22. V. Reshetnikov *et al.*, ROS-Responsive N-Alkylaminoferrocenes for Cancer-Cell-Specific Targeting of Mitochondria. *Angew Chem Int Ed Engl* **57**, 11943-11946 (2018).

23. H. J. Yoo *et al.*, Tumor-Specific Reactive Oxygen Species Accelerators Improve Chimeric Antigen Receptor T Cell Therapy in B Cell Malignancies. *Int J Mol Sci* **20**, (2019).
24. W. Chen, Y. Han, X. Peng, Aromatic nitrogen mustard-based prodrugs: activity, selectivity, and the mechanism of DNA cross-linking. *Chem. E. J.* **20**, 7410-7418 (2014).
25. H. Fan *et al.*, Assessment of Phenylboronic Acid Nitrogen Mustards as Potent and Selective Drug Candidates for Triple-Negative Breast Cancer. *ACS Pharmacol Transl Sci* **4**, 687-702 (2021).
26. Y. Wang *et al.*, Hydrogen peroxide activated quinone methide precursors with enhanced DNA cross-linking capability and cytotoxicity towards cancer cells. *Eur J Med Chem* **133**, 197-207 (2017).
27. T. C. Chou, P. Talalay, Quantitative analysis of dose-effect relationships: the combined effects of multiple drugs or enzyme inhibitors. *Adv. Enzyme Regul.* **22**, 27-55 (1984).
28. T. P. Chou TC, Analysis of combined drug effects: a new look at a very old problem. *Trends Pharmacol Sci* **4**, 450-454 (1983).
29. A. Ianevski, A. K. Giri, T. Aittokallio, SynergyFinder 3.0: an interactive analysis and consensus interpretation of multi-drug synergies across multiple samples. *Nucleic Acids Res* **50**, W739-W743 (2022).
30. M. A. Dymova, E. V. Kuligina, V. A. Richter, Molecular Mechanisms of Drug Resistance in Glioblastoma. *Int J Mol Sci* **22**, (2021).
31. A. Begleiter, M. Mowat, L. G. Israels, J. B. Johnston, Chlorambucil in chronic lymphocytic leukemia: mechanism of action. *Leuk Lymphoma* **23**, 187-201 (1996).
32. A. Koch *et al.*, Establishment of Early Endpoints in Mouse Total-Body Irradiation Model. *PLoS One* **11**, e0161079 (2016).
33. E. V. Paster, K. A. Villines, D. L. Hickman, Endpoints for mouse abdominal tumor models: refinement of current criteria. *Comp. Med.* **59**, 234-241 (2009).
34. P. T. Schumacker, Reactive oxygen species in cancer: a dance with the devil. *Cancer Cell* **27**, 156-157 (2015).
35. N. Shenoy, E. Creagan, T. Witzig, M. Levine, Ascorbic Acid in Cancer Treatment: Let the Phoenix Fly. *Cancer Cell* **34**, 700-706 (2018).
36. S. J. Padayatty *et al.*, Vitamin C: intravenous use by complementary and alternative medicine practitioners and adverse effects. *PLoS One* **5**, e11414 (2010).
37. J. Du, J. J. Cullen, G. R. Buettner, Ascorbic acid: chemistry, biology and the treatment of cancer. *Biochim. Biophys. Acta* **1826**, 443-457 (2012).
38. J. L. Welsh *et al.*, Pharmacological ascorbate with gemcitabine for the control of metastatic and node-positive pancreatic cancer (PACMAN): results from a phase I clinical trial. *Cancer Chemother. Pharmacol.* **71**, 765-775 (2013).
39. L. J. Hoffer *et al.*, High-dose intravenous vitamin C combined with cytotoxic chemotherapy in patients with advanced cancer: a phase I-II clinical trial. *PLoS One* **10**, e0120228 (2015).
40. Y. Ma *et al.*, High-dose parenteral ascorbate enhanced chemosensitivity of ovarian cancer and reduced toxicity of chemotherapy. *Sci Transl Med* **6**, 222ra218 (2014).
41. W. Wang *et al.*, CD8(+) T cells regulate tumour ferroptosis during cancer immunotherapy. *Nature* **569**, 270-274 (2019).
42. W. Wang *et al.*, Effector T Cells Abrogate Stroma-Mediated Chemoresistance in Ovarian Cancer. *Cell* **165**, 1092-1105 (2016).

43. T. Habtetsion *et al.*, Alteration of Tumor Metabolism by CD4+ T Cells Leads to TNF-alpha-Dependent Intensification of Oxidative Stress and Tumor Cell Death. *Cell Metab* **28**, 228-242 e226 (2018).
44. J. Tang, D. Ramis-Cabrer, X. Wang, E. Barreiro, Immunotherapy with Monoclonal Antibodies in Lung Cancer of Mice: Oxidative Stress and Other Biological Events. *Cancers (Basel)* **11**, (2019).
45. N. S. Aboelella *et al.*, Indomethacin-induced oxidative stress enhances death receptor 5 signaling and sensitizes tumor cells to adoptive T-cell therapy. *J Immunother Cancer* **10**, (2022).
46. N. S. Aboelella, C. Brandle, T. Kim, Z. C. Ding, G. Zhou, Oxidative Stress in the Tumor Microenvironment and Its Relevance to Cancer Immunotherapy. *Cancers (Basel)* **13**, (2021).